# Supporting Information

# Dry Transfer of van der Waals Crystals to Noble-Metal Surfaces to Enable Characterization of Buried Interfaces

Andrey Krayev[1], Connor S. Bailey[2], Kiyoung Jo[3], Shuo Wang[4], Akshay Singh[5], Thomas Darlington[6], Gang-Yu Liu[4], Silvija Gradecak[5], P.James Schuck[6], Eric Pop[2], Deep Jariwala[3]*

1. Horiba Scientific, Novato, CA 94949, USA
2. Department of Electrical Engineering, Stanford University, Stanford, CA, 94305, USA
3. Department of Electrical and Systems Engineering, University of Pennsylvania, Philadelphia, PA 19104, USA
4. Department of Chemistry, University of California, Davis, CA 95616, USA
5. Department of Materials Science and Engineering, Massachusetts Institute of Technology, , Cambridge, MA, 02139 USA
6. Department of Mechanical Engineering, Columbia University, New York, NY, 10027, USA

*Corresponding Author. Email: dmj@seas.upenn.edu

## 1. Materials Synthesis, Deposition, and Sample Preparation:

### Chemical Vapor Deposition of $WSe_2$

The synthetic monolayer $WSe_2$ grains were grown in a method similar to that shown for $MoSe_2$ monolayers previously.[1] Growth substrates, in this case thermally grown $SiO_2$ on Si, were treated with HMDS and decorated with perylene-3,4,9,10 tetracarboxylic acid tetrapotassium salt (PTAS) to act as a seeding promoter. The main motivation behind the HMDS treatment of our growth substrates specifically stems from our use of perylene-3,4,9,10 tetracarboxylic acid tetrapotassium salt (PTAS) as a seeding promoter. PTAS is a fairly common treatment for CVD growth of TMDs, usually applied as an aqueous solution. We have found that applying the PTAS as small droplets around the edge of our chip results in better TMD growth with a cleaner interface to the substrate.[2] These droplets are baked and evaporated to remove excess liquid prior to growth, which results in any impurities in the solution depositing as "coffee rings". In order to maximize our usable area and minimize the size of these "coffee rings", we utilize an HMDS treatment to make the surface of our substrate hydrophobic, which makes the applied aqueous PTAS droplets smaller. In summary, the use of HMDS does not directly motivate or improve our TMD growth, but practically allows for more growth on a chip without impacting material or electrical quality.

A two-zone quartz tube furnace was loaded with approximately 100 mg of selenium pellets in the first zone and 25 mg of $WO_3$ in the second, downstream, zone. The treated substrate was placed directly downstream from the $WO_3$ powder. Under 60 sccm argon flow at atmospheric pressure, the selenium zone was heated to 500°C and the $WO_3$ zone to 900°C, at which point a 9 sccm flow of $H_2$ was introduced to aid in reduction of the reaction. After 25 minutes, the $H_2$ flow was removed and the furnace temperature was ramped down to ambient. These conditions result in direct monolayer growth of $WSe_2$ with grain sizes on the order of dozens of microns.

## Chemical Vapor Deposition of $MoS_2$

The monolayer $MoS_2$ growth is carried out at atmospheric pressure in an inert environment (argon). Before the growth is carried out, the 1" CVD tube is heated to ~ 200°C, with continuous evacuation and argon flow for ~ 30 min, to clean the tube of water and other impurities. Subsequently, the tube is brought up to atmospheric pressure with argon. The precursors (sulfur ~ 1 gm and molybdenum oxide powder ~ 20 mg) are kept in alumina boats (in the first and second zones respectively). The substrate (silicon dioxide/ silicon) is kept on top of the boat containing $MoO_3$ powder (facing down). The flow rate of argon carrier gas is kept at 50 sccm, optimized for single layer growth. The furnace is heated at a rate of 25°C/min with temperature of first (T1) and second (T2) zones targeted at 400°C and 800°C, respectively. After both zones reach the set temperatures, the sulfur boat is pushed to the edge of zone 1 using a pair of magnets, and growth is carried out for 10 min. Subsequently, the tube is gradually brought down to room temperature at a typical rate of 10°C/min.

## Gold/Silver Deposition

### Thermal gold or silver deposition

100 nm Au or 55 nm Ag thin film was deposited in a high-vacuum evaporator (model DV502-A, Denton Vacuum Inc., Moorestown, NJ). For the Ag thin film, 50 nm Au was successively deposited to prevent Ag oxidation. The Au or Ag was thermally vaporized and deposited onto as-synthesized samples at room temperature and under a base pressure of $5.1 \times 10^{-6}$ Torr. The evaporation rate was monitored by a quartz crystal monitor (Inficon Inc., East Syracuse, NY) and controlled between 0.10 and 0.15 nm/s. After the deposition, the sample was immediately removed from the chamber and ready for the next step treatment.

### Gold sputtering

Gold is sputtered using a EMS Q150T ES coater at low pressures ($5 \times 10^{-5}$ mbar). The rate of deposition is 15 nm/min Au with a sputter current of 20 mA, and a total film thickness of 20 nm.

### Electron beam deposition of Au

100 nm Au was deposited using e-beam evaporator (model Lesker PVD75 E-beam Evaporator). The deposition rate was 0.1 nm/s, controlled by QCM under a base pressure of $5\times 10^{-7}$ Torr.

## Mechanical Exfoliation and Template Stripping:

Mono- and few-layered $WSe_2$ flakes were deposited on $SiO_2$ (300 nm) on Si substrates by mechanical exfoliation technique in the glove box ($H_2O$, $O_2 < 0.5$ ppm) using a Scotch Tape. The substrate was prebaked in the glove box to avoid possible water traps. After careful flake selection, 100 nm Au was deposited using e-beam evaporation. Using two-component epoxy, the Au layers were fixed to transfer substrate and flipped.

## 2. Extended Data on CVD grown $WSe_2$:

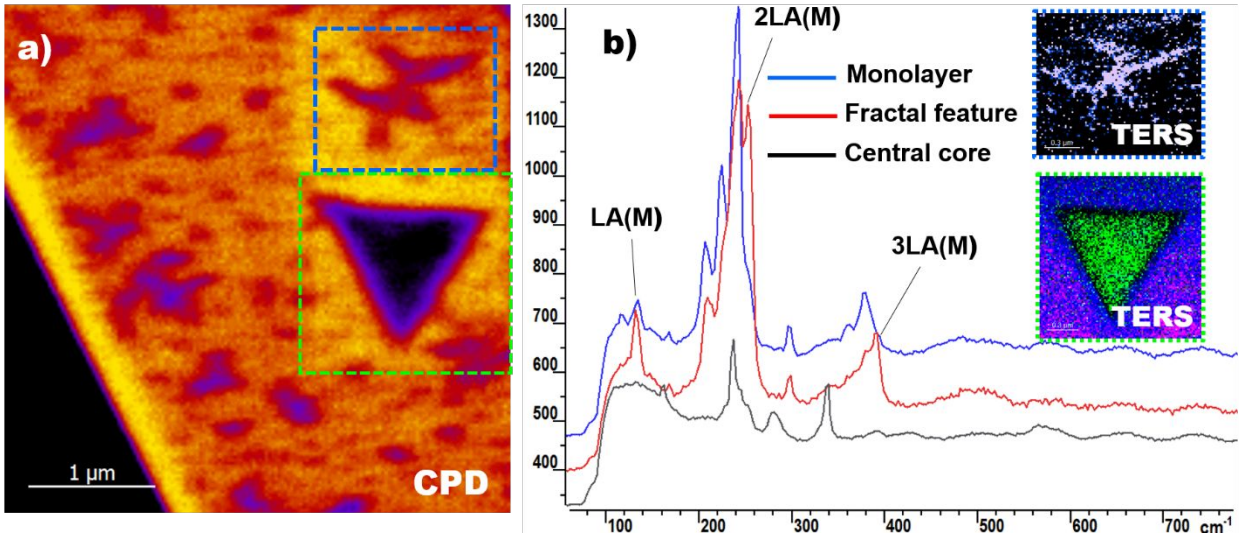


**Figure S1. a) CPD image of a gold-transferred $WSe_2$ crystal from Fig. 2 in main text. TERS maps were collected in the blue and green dotted boxes, featuring lower CPD fractal feature and central triangular core in blue and green boxes respectively. b) averaged TERS spectra from the core (black), monolayer area (blue) and fractal feature (red); spectra are offset vertically for clarity. Upper inset — TERS map (peak position of complex peak in 200 $cm^{-1}$ to 265 $cm^{-1}$ range of red spectrum) of the fractal feature; lower insert- TERS map ( peak intensity of 336 $cm^{-1}$ peak (green), complex peak in 200 $cm^{-1}$ to 265 $cm^{-1}$ range (blue) and complex peak centered at 380 $cm^{-1}$ (red)). Both the fractal structure and the central core, both of which show decreased CPD, also have quite different Raman response from the adjacent monolayer.**

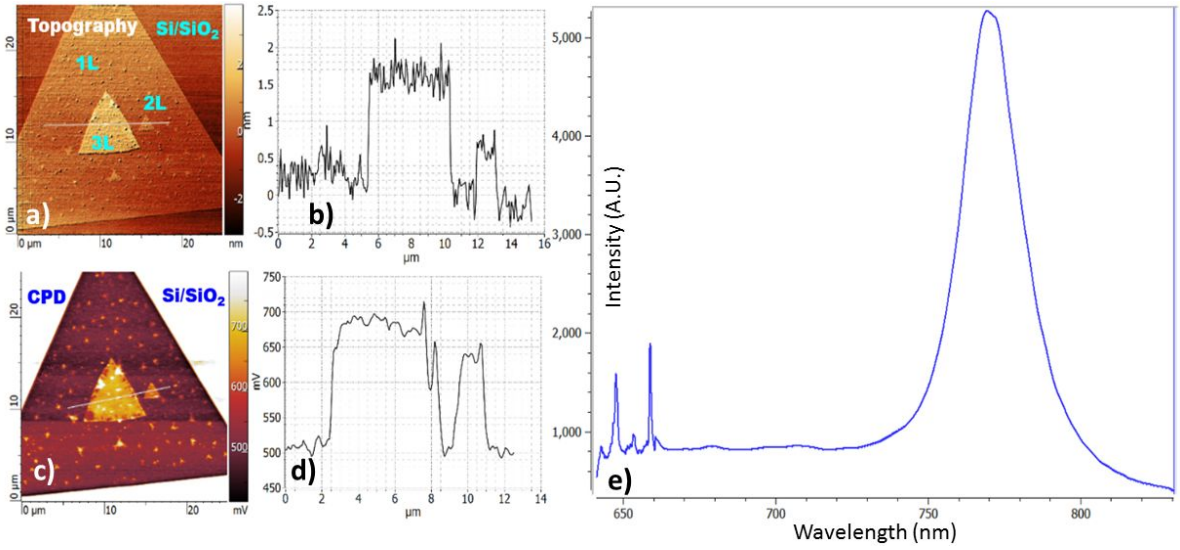


**Figure S2. a) topography image and b) corresponding section analysis of as-grown WSe2 crystal with a central trilayer and a number of bilayer islands; c) CPD image and d) corresponding section analysis; e) – Raman and photoluminescence (PL) spectrum from a location on monolayer part of the crystal showing high PL intensity for monolayer.**

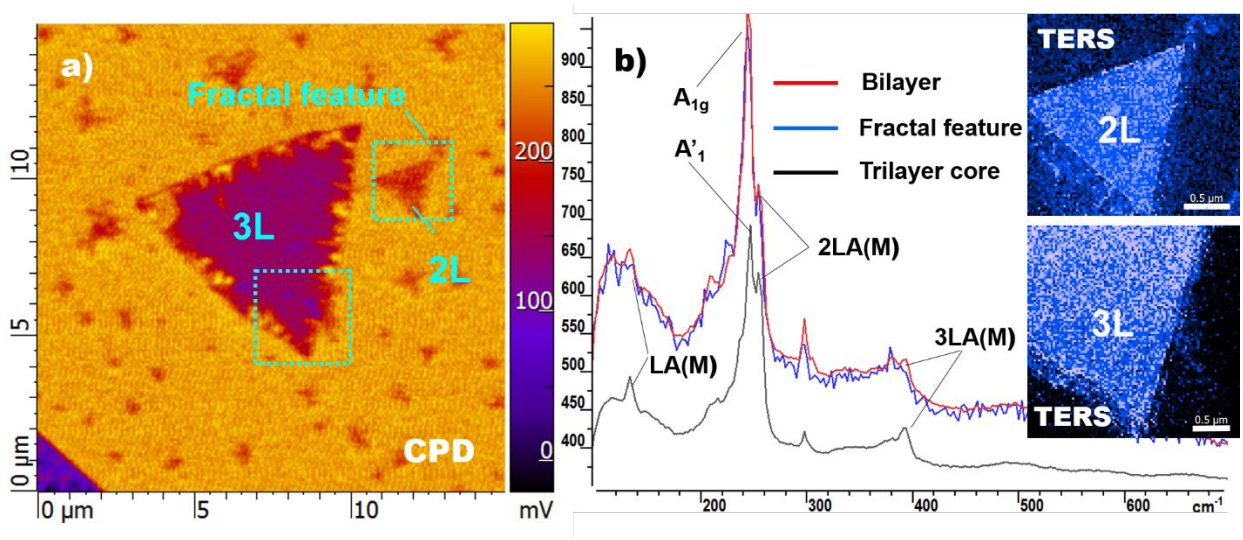


**Figure S3. a) Digital zoomed-in CPD image of the crystal in Fig. 3 of main text after gold transfer. TERS maps were collected over the areas marked with blue dotted boxes marked with blue dotted boxes b)averaged TERS spectra from bilayer(red), fractal bilayer feature (blue) and trilayer core (black). As can be clearly seen from these spectra, relative intensity of the 2LA(M) peak compared to $A_{1g}$ peak is practically identical for the triangular and fractal bilayer features, while it increases for the trilayer core. In the insert- TERS maps (peak position of the complex peak within 230-270 $cm^{-1}$ range.**

## 3. Characterization and analysis of CVD grown $MoS_2$ samples:

In the first series gold layer was deposited on $MoS_2$ crystals via sputtering, the rest of the transfer procedure was the same as in case of $WSe_2$. $MoS_2$ crystals were successfully transferred from the growth substrate, featuring very shallow roughness of the surface and familiar concentric triangular features with lower value of the surface potential in the CPD images of some $MoS_2$ crystals (Fig. S4). Despite the similarity of the sample surface morphology and CPD distribution to the case of gold-assisted transfer of $WSe_2$, TERS map of the of $MoS_2$ crystal showed almost negligible Raman response from the monolayer areas and only fairly weak $A_{1g}$ and $E_{2g}$ peaks intensity over the central triangular feature. This was specifically surprising taking into account high background signal in TERS spectra, which was an indication of strong enhancement of the TERS probe.

To clarify the reasons of such poor TERS performance of gold –assisted transferred $MoS_2$ crystals, we repeated the experiment, this time depositing gold via thermal evaporation following the same protocol and using exactly the same deposition system that was used for experiments with $WSe_2$ crystals. Transfer of these samples was also successful, and though there were some pits on the exposed gold surface, they did not affect our ability to perform SKM and TERS characterization.

SKM characterization of the sample showed some significant differences in the CPD signal across the transferred flake, though the contrast was not as sharp as in case of $WSe_2$. The TERS map collected over the internal part of the flake that featured significant variation of the CPD value (Fig. S5), featured high quality TERS spectra with strong signal-to noise ratio and showing presence of multiple resonant peaks in addition to $A_{1g}$ and $E_{2g}$ modes. Major variations in TERS

spectra were related to the intensity of the background and the intensity of complex resonant modes LA(~K)+TA(~K), following the peak assignment of Carvalho *et al*.[2] at around 423 $cm^{-1}$.What was specifically interesting was that the TERS map of the peak position for 380-440 $cm^{-1}$ spectral range showed reasonably good correlation with the CPD image. On the other hand, the map representing both the Raman peak and the background intensity (peak area) clearly showed a triangular shaped feature in the upper portion of the flake. This feature did not have a corresponding counterpart in the CPD image. Further, a number of small 100-200 nm "bubble-like" features showing increased intensity of both the Raman peaks and the background were observed as seen in Fig. S6. This observation again highlights the power of TERS imaging that can reveal features unobservable otherwise.

Overall, we must conclude that while the gold –assisted transfer of $MoS_2$ was possible in principle, SKM and TERS data obtained on transferred crystals were not as clear and unambiguous as for $WSe_2$. This could likely be due to presence of some growth-specific "contamination" layer between the $MoS_2$ crystals and the $SiO_2$/Si substrate which prevents direct access to the tip and will have to be clarified in a follow-up study.

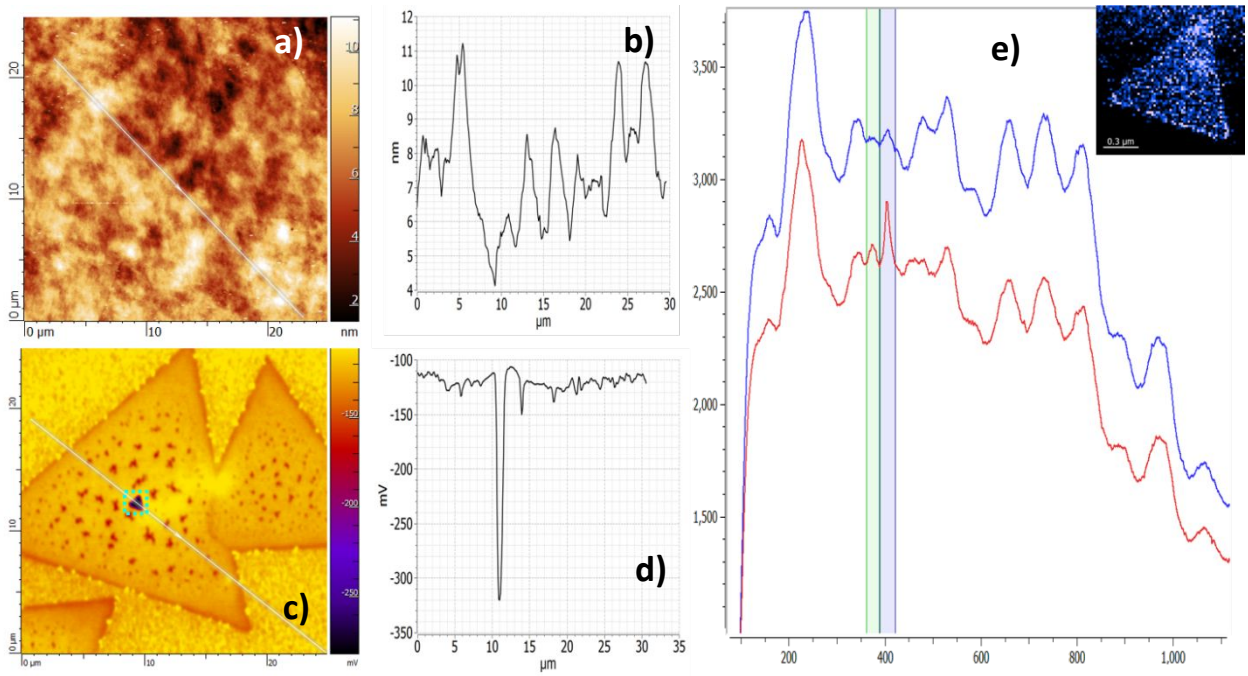


**Figure S4. a) Topography of the $MoS_2$ sample transferred with sputtered gold; b) corresponding section analysis; c)- CPD image of the same area showing a signature of thicker triangular core in the center of bigger crystal; d)- corresponding section analysis showing significant (over 150 mV) drop of the surface potential over the central core; e)- TERS map ( intensity of 408 $cm^{-1}$ peak) collected over the dotted square in c) and typical spectra from the monolayer (blue) and central core ( red).**

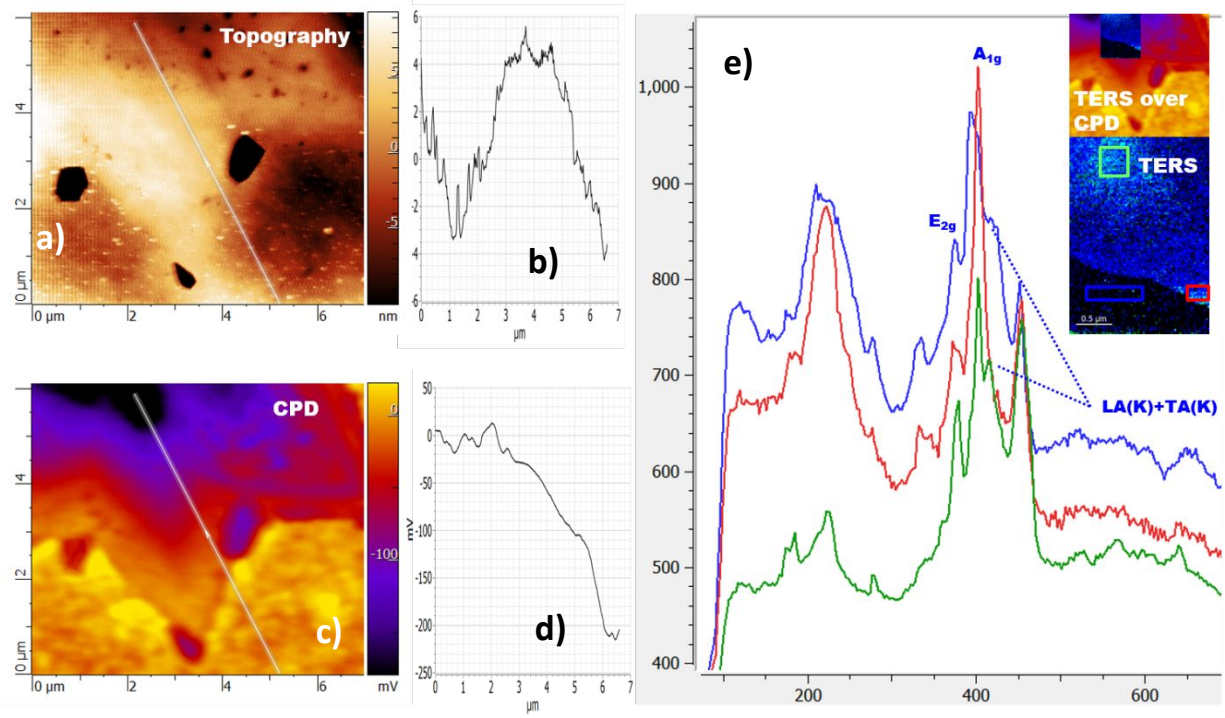


**Figure S5. a) topography of $MoS_2$ sample transferred with thermally evaporated gold; b)-corresponding section analysis; c)- CPD image of the same area; d) –section analysis of the CPD image; e) averaged TERS spectra and corresponding TERS maps ( 380-440 $cm^{-1}$ peak position) with color coded boxes (inset) showing very sharp borderlines, which additionally confirms near-field nature of the recorded signal. (Units: x axis: Wavenumber ($cm^{-1}$), y axis: Intensity (A.U.))**

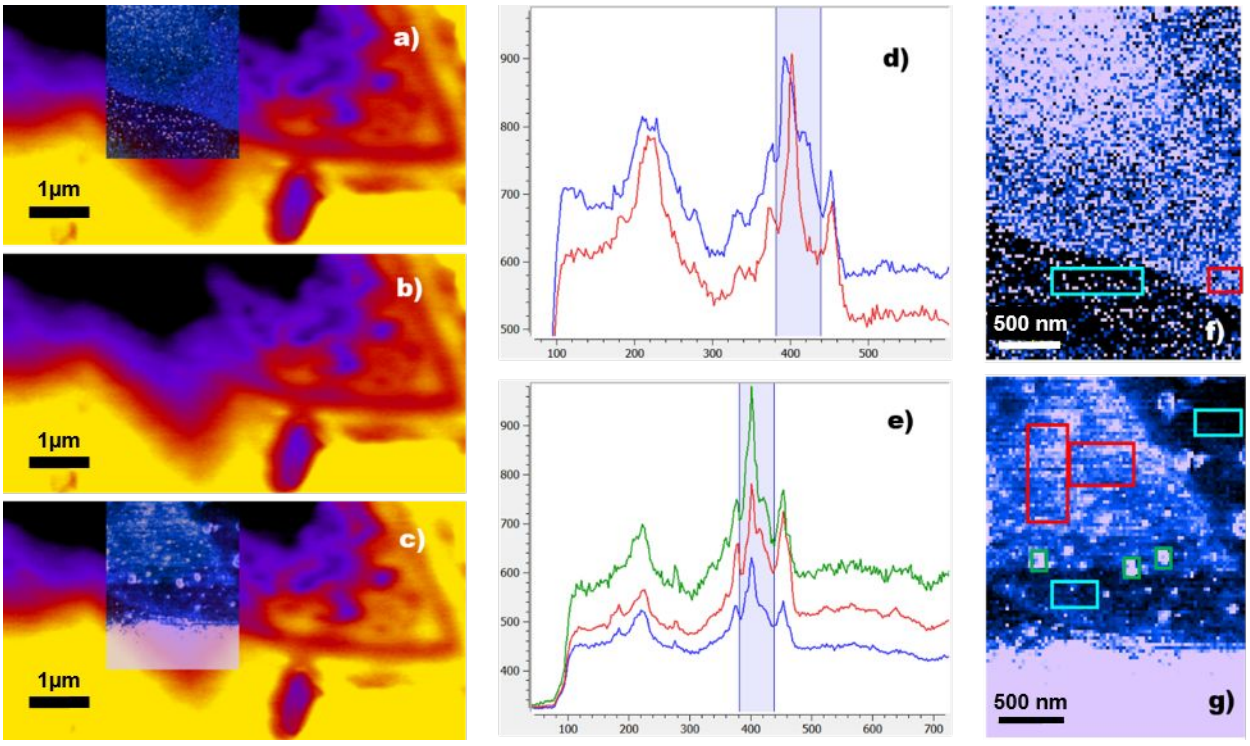

**Figure S6. $MoS_2$ sample transferred with thermally evaporated gold. Same area as in Fig.S5. a)-TERS map (380-440 $cm^{-1}$ peak position) overlaid over CPD; b) corresponding CPD image; c) TERS map (380-440 $cm^{-1}$ peak area including background) overlaid over CPD. A sharp triangular feature is clearly seen in this map that does not have a counterpart in the CPD image; d) averaged TERS spectra from correspondingly colored areas in f); e) averaged TERS spectra from correspondingly colored areas in g); f)- TERS map (380-440 $cm^{-1}$ peak position); g) TERS map of the same area representing 380-440 $cm^{-1}$ peak area including background.**

## 5. CPD and TERS mapping of Au-transferred direct exfoliated $WSe_2$

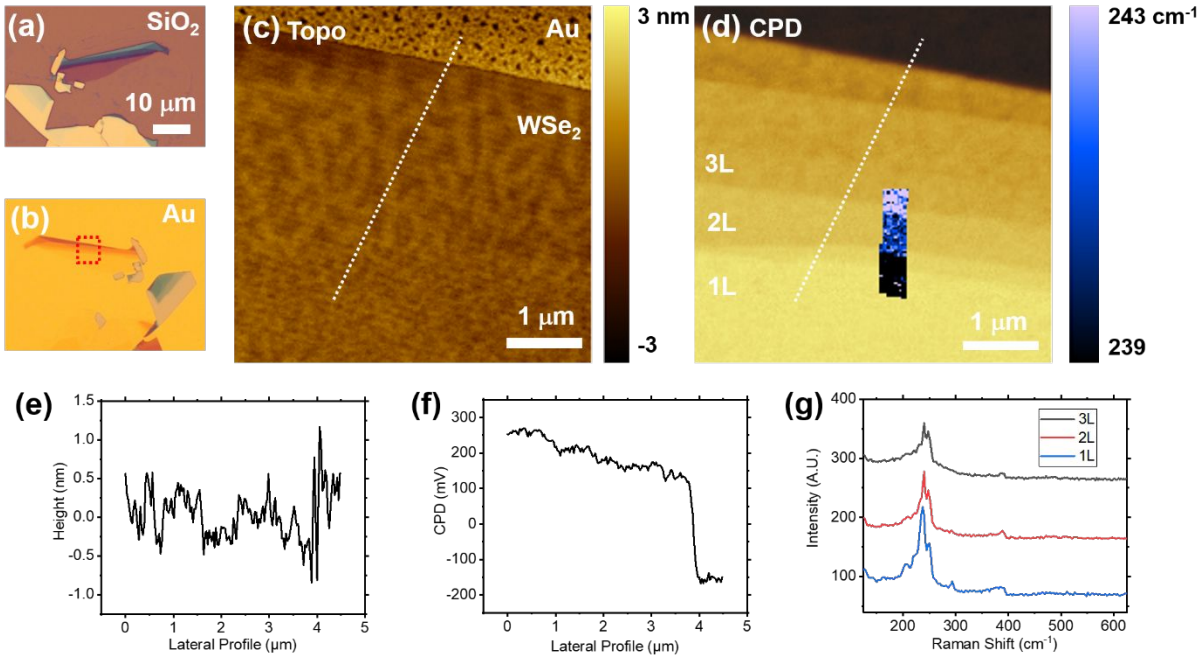


**Figure S7. Optical Image of (a) direct exfoliated $WSe_2$ on $SiO_2$/Si and (b) Au-transferred $WSe_2$ original flake. (c) Topography and (d) CPD of highlighted red box region in (b) and corresponding lateral profile of (e) topography, (f) CPD. Blue box in (d) is TERS peak position mapping. (g) TERS spectrum corresponding to (d).**

## 6. Far-Field Raman Spectra

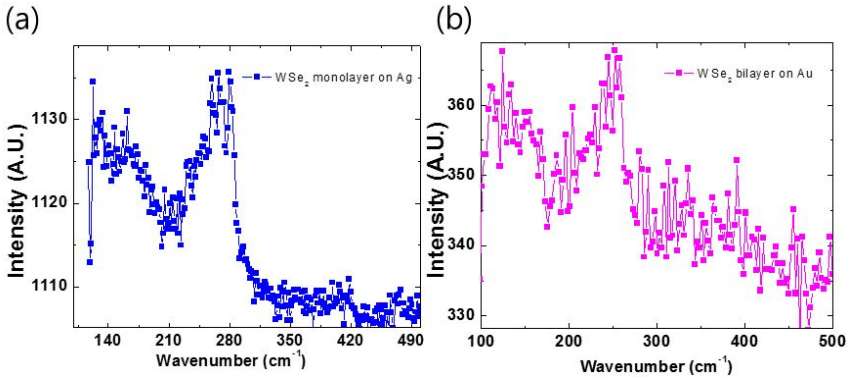


**Figure S8. (a) Far-field Raman spectrum of CVD grown monolayer $WSe_2$ flake on Ag. No clear Raman signal is evident in comparison to near-field signals in Figure 3 and 4 of main manuscript (b) Far-field Raman**

**spectrum of CVD grown monolayer $WSe_2$ flake on Ag. No clear Raman signal is evident in comparison to near-field signals in Figure 3 and 4 of main manuscript thereby rendering comparison difficult.**

# References:


1. Smithe, K. K. H.; Krayev, A. V.; Bailey, C. S.; Lee, H. R.; Yalon, E.; Aslan, Ö. B.; Muñoz Rojo, M.; Krylyuk, S.; Taheri, P.; Davydov, A. V.; Heinz, T. F.; Pop, E. Nanoscale Heterogeneities in Monolayer $MoSe_2$ Revealed by Correlated Scanning Probe Microscopy and Tip-Enhanced Raman Spectroscopy *ACS Applied Nano Materials,* **2018**, 1, 572-579.

2. Kirby K H Smithe, Chris D English, Saurabh V Suryavanshi and Eric Pop, Intrinsic Electrical Transport and Performance Projections of Synthetic Monolayer $MoS_2$ Devices. *2D Materials,* **2017**, 4 011009

3. Carvalho, B. R.; Wang, Y.; Mignuzzi, S.; Roy, D.; Terrones, M.; Fantini, C.; Crespi, V. H.; Malard, L. M.; Pimenta, M. A. Intervalley Scattering by Acoustic Phonons in Two-Dimensional $MoS_2$ Revealed by Double-Resonance Raman Spectroscopy**.** *Nature Communications* **2017,** 8, 14670.